Available online at www.sciencedirect.com
ScienceDirect
Surface Science 601 (2007) 3020–3033
SURFACE SCIENCE
www.elsevier.com/locate/susc

NH_3 on Si(001): Can Gaussian cluster and planewave slab models agree on energetics?

O. Warschkow *, T.L. McDonell, N.A. Marks

Centre for Quantum Computer Technology, School of Physics, The University of Sydney, Sydney 2006, NSW, Australia

Received 5 December 2006; accepted for publication 4 May 2007
Available online 24 May 2007

Abstract

We critically evaluate the use of cluster and periodic slab models in describing the NH_3/Si(001) molecule–surface reaction system. We show that considerable discrepancies in the relative adsorbate energetics originate in the limitations of the small cluster and slab models commonly used. These limitations in turn are the consequence of the balance that must be struck between the competing demands of cluster/slab size, basis set size and exchange–correlation model. This leads us to consider "cluster compound models" in which the results of several smaller calculations (separately probing the effects of cluster/slab size, basis set size and exchange–correlation model) are combined to estimate the energy of a converged model.

Keywords: Density functional calculations; Energetics; Silicon (001) surface; Ammonia

1. Introduction

The reactive interaction of molecules with surfaces is at the heart of many technological processes, including catalysis, epitaxial growth of materials, corrosion and nanotechnology. Complementary to experimental surface science techniques such as scanning-probe microscopy, temperature programmed desorption, and assorted spectroscopies, detailed insights into reaction intermediates and mechanisms may be obtained by first-principles theory (see e.g. Refs. [1–4]). The utility of theory however is critically dependent on the quality and accuracy of the surface-chemistry model. Models of lesser accuracy may still provide valuable qualitative insights into the reactivity of a molecule with a surface. Being less expensive computationally such models can be applied to a larger number of possible reaction intermediates and thereby help establish the "big picture". However, when detailed reaction rates are required in order to understand complex dynamical behaviour, a higher level of accuracy in energy calculations is warranted for. In this work we consider the reaction of ammonia (NH_3) with the Si(001) surface and illustrate the difficulties (and limits) of achieving high accuracy in computational models of molecules on surfaces. Of considerable relevance to the semiconductor industry in the fabrication of Si_3N_4 dielectric films [5], this reaction has been the subject of a number of computational studies [6–20] aimed at elucidating the elementary chemical steps in the dissociation pathway. Close inspection of these works (see Table 1) however reveals a surprising degree of disagreement in the relative energetics of various intermediate reaction species. In this work we ask the question how do these disagreements come about and what do they tell us about our ability to reliably model the chemistry of molecules on surfaces?

Calculations of molecule/surface systems broadly fall into two categories: cluster-based methods, which are popular in the quantum chemistry community, and periodic slab methods, which originate from condensed matter physics. A principal difference rests with the choice of basis sets, with cluster calculations generally using atom-centered Gaussian-type functions, while slab models are typically based on a planewave expansion. It is clear from

* Corresponding author. Tel.: +61 2 9036 9085; fax: +61 2 9351 7726.
E-mail address: oliver@physics.usyd.edu.au (O. Warschkow).

0039-6028/$ - see front matter © 2007 Elsevier B.V. All rights reserved.
doi:10.1016/j.susc.2007.05.017

Table 1
Binding energies of selected dissociation intermediates of NH_3 on Si(001) as reported in the literature

Reference	Model	A1	B1	B6	B10	C5	C10	G1
Xu et al. [6,7]	Cluster (1-dimer)	−0.94	−2.30	−1.36	−1.32	−2.82	−2.78	−3.26
Widjaja et al. [8]	Cluster (1-dimer)	−1.13	−2.21	−1.21	−0.61	−2.47	−1.82	−1.34
McDonell et al. [9]	Slab (2 × 4)	−1.48	−2.25	−1.52	−1.10	−2.67	−2.44	–
Kim and Cho [10]	Slab (2 × 2)	−1.27	−1.96	–	–	−2.25	−1.70	−1.47
Lu and Lin [4]	Cluster (1-dimer)	−1.05	−2.41	−1.52	–	–	–	–
Fattal et al. [11]	Cluster (1-dimer)	−1.43	−3.25	–	–	–	–	–
Widjaja et al. [12–14]	Cluster (3-dimer)	−1.26	−2.21	–	–	–	–	–
Widjaja and Musgrave [13]	Cluster (5-dimer)	−1.26	−2.17	–	–	–	–	–
Miotto et al. [15]	Slab (1 × 2)	−1.08	−2.45	–	–	–	–	–
Lee and Kang [16]	Slab (2 × 2)	−1.21	−1.99	–	–	–	–	–
Chung et al. [17]	Slab (4 × 8)	−1.31	−2.06	–	–	–	–	–
Owen et al. [18]	Slab (2 × 4)	−1.36	−2.04	–	–	–	–	–
Lee and Cho [19]	Slab (2 × 4)	−1.29	−1.98	–	–	–	–	–

The chemical structures corresponding to the alphanumeric structure identifiers (A1, B1, B6, etc.) are shown in Fig. 1. All energies have been converted to eV and are given relative to the energy of gas phase NH_3 and the free surface. For cluster model results, we indicate the number of surface Si–Si dimers that were used. For slab models, we give the periodic surface unit cell. A (1 × 2) cell corresponds to a single Si–Si dimer.

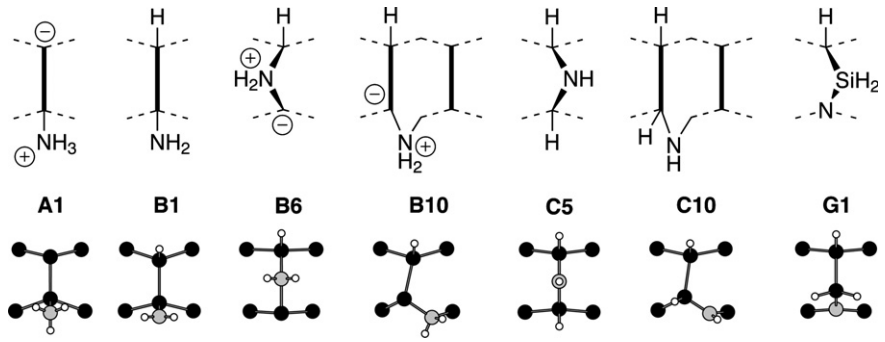

Fig. 1. Three-dimensional (on-top) view and schematic valence structure diagram of the seven NH_3/Si(001) dissociation intermediates considered in this work. Silion, hydrogen and nitrogen atoms are colored black, white and grey, respectively. The labelling of the structures follows the notation used in Ref. [9] where A-type structures contain the NH_3 moiety, B-type structures contain NH_2, etc.

Table 1 that considerable scatter exists in both the cluster- and slab-based calculations, at times leading to qualitatively different structural orderings. While one would intuitively expect that cluster and slab models could be brought to numerical agreement, restrictions in computational resources impose limits on the size of the calculations which may be performed. Going considerably beyond cluster/slab sizes typically employed in surface theory work, we enquire here to what degree cluster and slab models can agree on energetics.

We will examine here the four principal sources of computational error in molecule–surface interactions. (1) *Finite model size*: in cluster calculations, a finite number of atoms is used to represent the surface. This limits the degree to which the cluster may relax and respond to strains induced by surface adsorption/dissociation processes. The size of the cluster, the termination of truncated bonds between cluster and the remainder of the crystal, and any constraints applied, all introduce errors into calculated binding energies. Analogous errors arise in slab models, where the surface is represented by a finite number of atoms together with a periodic repeat. The repeat from one cell into the next introduces constraints that also limit the ability of the surface to relax. Further errors can arise from electrostatic and steric interactions between the adsorbate and its periodic images. (2) *Finite basis sets and pseudopotentials*: in Gaussian cluster models, the increase in basis set comes at considerable computational expense and is far from straightforward, requiring typically a balanced increase in number of split-valence, split-core, polarization and diffuse functions. In planewave slab calculations, basis effects are under tight control via a single parameter, the kinetic energy cutoff. In the latter models it is common practice to determine the cutoff such that the computed properties of interest are converged. Instead the basis set error emerges indirectly through the choice of pseudopotential that is often designed so as to present a balance between accuracy (hard potentials, requiring larger cutoffs, i.e. more basis functions) and computational efficiency (soft potentials, permitting smaller cutoffs, i.e. fewer basis functions). (3) *Approximate exchange–correlation*: we focus here primarily on DFT methods for which the local density approximation (LDA), the generalized gradient approximation (GGA) and exact-exchange functionals describe three levels of increasing energetic accuracy and computational expense. (4) *Zero point vibrational energies* make a small but

significant contribution to calculated binding energies. Zero-point corrections tend to be more commonly applied in surface cluster models, perhaps due to the ready availability of analytical second derivatives of the energy in these models.

In the following we will be using the seven NH_3 adsorption structures in Table 1 as trial structures and examine how their binding energies are affected by the four computational aspects enumerated above. We stress however, that it is not the purpose of this present work to reinterpret the NH_3/Si(001) surface chemistry. Instead this work intends to provide guidelines and recommendations for the abilities and limits of typical cluster and slab model that are currently being used. Taking cues from compound models in gas-phase quantum chemistry (e.g. the G2 [21] and CBS [22,23] model chemistries) and similar models developed for the H_2/Si(001) reaction [24–27], we consider how by combining the results of a series of calculations one may achieve higher levels of accuracy. These guidelines should be of wider relevance to reactivity studies of other molecules on the Si(001) surface.

2. Computational methodology

For our discussion of cluster-size convergence, we define five series of cluster representations of the surface (tiny, small, large, extra-large and extra-wide) as illustrated in Fig. 2. Each series is composed of a basic cluster type of a certain width and depth that is extended in length, that is, in the number of surface Si–Si dimers. The series of *tiny* clusters Fig. 2a is based on the Si_6H_{12} 1-dimer cluster, which comprises the two Si atoms of the dimer and four Si atoms in the layer below. Extension of this cluster to 2-, 3-, 4- and 5-dimer clusters leads to stoichiometries $Si_{10}H_{16}$, $Si_{14}H_{20}$, $Si_{18}H_{24}$, and $Si_{22}H_{28}$, respectively. The series of *small* clusters Fig. 2b is based on the Si_9H_{12} 1-dimer cluster, which contains 2, 4, 2 and 1 Si atoms in first to fourth surface layers, respectively. The 2- to 7-dimer higher analogues have the stoichiometry $Si_{15}H_{16}$, $Si_{21}H_{20}$, $Si_{27}H_{24}$, $Si_{33}H_{28}$, $Si_{39}H_{32}$, $Si_{45}H_{36}$. The series of *large* clusters Fig. 2c is based on the $Si_{17}H_{22}$ 1-dimer cluster constructed from 2, 4, 6, 3 and 2 atoms in first to fifths surface layers, respectively. This leads to $Si_{29}H_{32}$, $Si_{41}H_{42}$, $Si_{53}H_{52}$, $Si_{65}H_{62}$ stoichiometries for two to 5-dimer cluster models, respectively. In order to further test the convergence of calculated energies with respect to cluster width/depth, we performed two additional sets of calculations: The *extra-large* cluster $Si_{63}H_{73}$ Fig. 2d is three dimers long and contains an additional layer of Si atoms extending the 3-dimer/large cluster Fig. 2c in width and depth. The *extra-wide* cluster $Si_{89}H_{60}$ Fig. 2e is three dimers long and extends the 3-dimer/large cluster Fig. 2c in width only, adding a complete additional dimer-row of three dimers on either side of the centre dimer-row. The extra-wide cluster is the only cluster in our set that includes adjacent dimer rows and will help us probe interactions of the surface-bonded molecule with adjacent rows.

We follow the general practice to use hydrogen atoms to terminate the dangling bonds that arise when a finite-sized cluster is used to represent an extended surface. In our calculations, the positions of these terminating hydrogen atoms are held fixed during all geometry optimisations so that they provide an *ad hoc* representation of the strain induced by the surrounding surface atoms not explicitly included in the cluster model. We determine the position of these terminating atoms using a fully relaxed slab model of a monohydride-terminated Si(001) surface as a template.[1] We identify within this template structure the Si–Si bonds that are broken in the formation of the cluster and place terminating hydrogen atoms along the broken bonds such that the resulting Si(cluster)–H bond is 1.49 Å.[2] The same placement of terminating hydrogen atoms is used in the relaxation of all seven trial structures (and the free surface). While the terminating hydrogen remain fixed during geometry optimisations, all Si and adsorbate atoms are fully relaxed.

Calculations on cluster models with Gaussian-type-orbital basis sets were performed using the *Gaussian 03* software [28] together with PW91 GGA [29,30] and the B3LYP hybrid exact-exchange functionals [31,32]. In our discussion we will examine the role of different Gaussian-type basis sets on calculated binding energies, where, for reasons of computational economy, we place a proportionally larger number of basis functions on the surface nearest atoms that are most directly involved in the adsorption/dissociation process. These composite basis sets, labelled A to E in order of increasing size, accuracy and computational expense, are defined in Table 2.

The planewave/pseudopotential calculations on surfaces were performed using the *VASP* software [36–40] in the PW91 generalized-gradient approximation [29,30] to density functional theory. In the planewave/pseudopotential representation, a surface is represented using slab models that are 3-dimensionally periodic; in addition to the 2D in-plane periodicity of a single slab, the out-of-plane

[1] We use a monohydride terminated Si(001) surface as a template because the Si–Si surface dimers are symmetric in this structure which leads to cluster-terminating H-atom positions that are equally symmetric. This is an important detail because it ensures that the cluster-termination does not impose a bias on any symmetry breaking processes; e.g., the direction of dimer buckling when the cluster is used to describe the free surface. The hydrogen-terminations for the tiny, small and large cluster series have been constructed using the six Si-layer surface slab that is discussed in the planewave/pseudopotential calculations (PW91-GGA, US-1 potential, see text). For the hydrogen-termination of the extra-large and extra-wide cluster a thicker slab model of 25 Si-layers was used as a template.

[2] The Si–H bond lengths used to place the terminating hydrogen atoms for cluster and slab models are ad hoc choices: for the cluster model termination, we use 1.49 Å, which is the calculated Si–H bond length of silane (SiH_4) at the PW91/6-311G(d,p) level (1.4944 Å) rounded to two decimal places. For the dihydride termination of the slab models, we use a shorter bond length of 1.46 Å to reduce the proximity between hydrogen atoms on adjacent SiH_2 groups. In order to absorb the strain induced by this termination, the terminated silicon atoms of the slab model are held constrained at bulk positions.

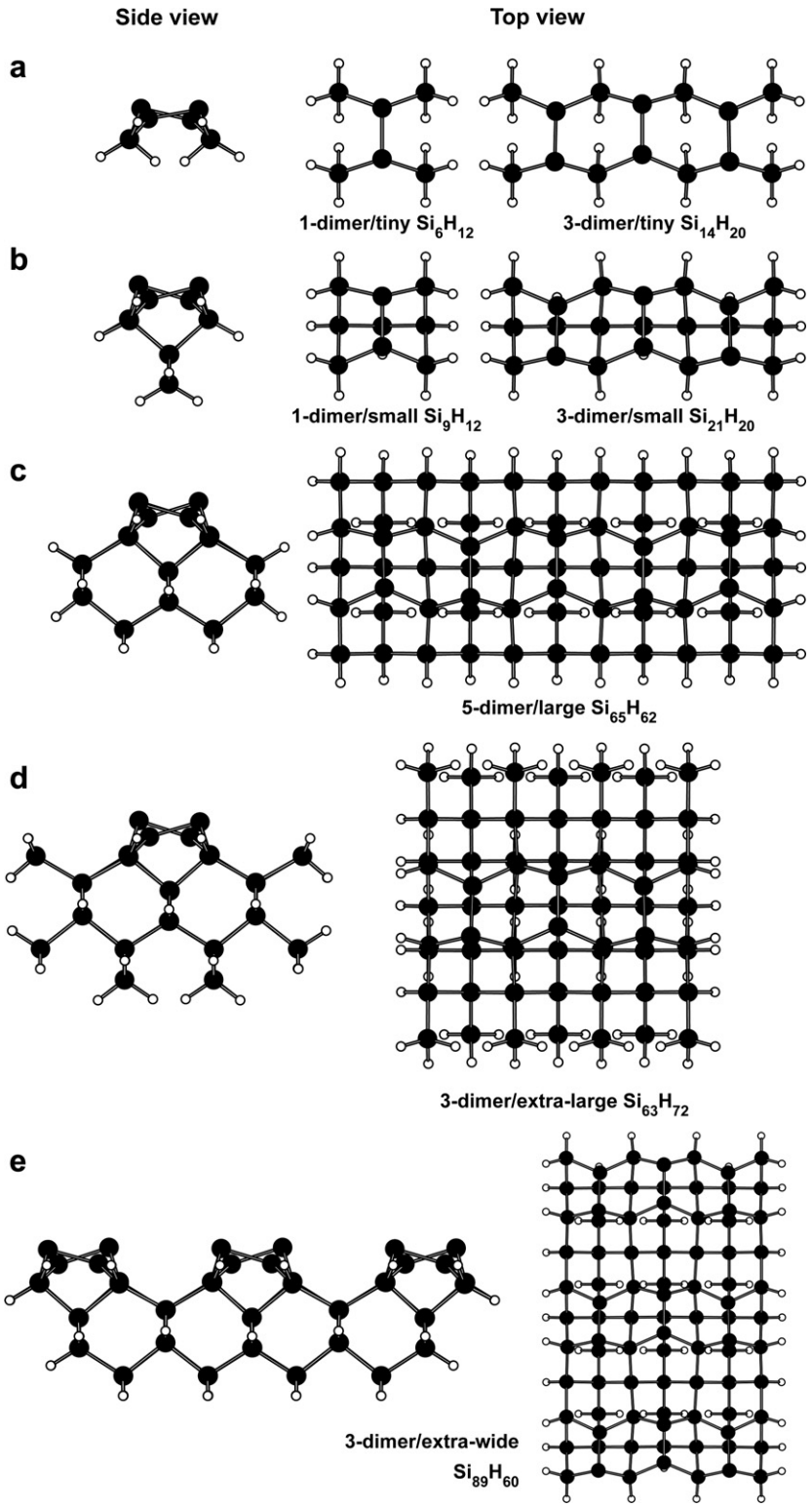

Fig. 2. Overview of cluster models used in this work. Five cluster series (a) *tiny*, (b) *small*, (c) *large*, (d) *extra-large* and (e) *extra-wide* differ in the width and depth of the cluster as illustrated in the side views along the dimer row. Within each series clusters differ in the number of surface dimers. Top-views of one-, three- and five-dimer cluster models are shown on the right-hand side.

periodicity leads to a succession of finite-sized slabs that are separated from each other by a vacuum gap (as illustrated in Fig. 3a). All slab calculations reported here utilize a surface model of six atomic layers of Si (including the surface dimer-layer) and a rigid "dihydride-like" termination of the dangling bonds on the opposite slab-surface that is not used for adsorption. This dihydride termination involves the Si-atoms in the layer furthest from the reactive

Table 2
Hierarchy of composite Gaussian type basis sets used in this work. In order to be economical with the basis set size, larger (more accurate) atomic basis sets are applied to adsorbate atoms (N + 3H) and Si atoms closest to the surface

	Adsorbate and first (dimer) layer atoms	Second layer atoms	Third and higher layer atoms and H-termination
Basis set A	6-311++G(d,p)	6-311G(d,p)	LANL2DZ
Basis set B	6-311++G(d,p)	6-311G(d,p)	6-311G(d,p)
Basis set C	6-311++G(2df,2pd)	6-311G(2df,2pd)	6-311G(2df,2pd)
Basis set D	AUG-cc-pVQZ	6-311G(2df,2pd)	6-311G(2df,2pd)
Basis set E	AUG-cc-pVQZ	cc-pVQZ	cc-pVQZ

Note that the cc-pVQZ basis set used in sets D and E contains polarization functions of (3d2fg, 3p2df) quality, i.e. one level of angular momentum higher than set C. Additional calculations conducted using the more compact cc-pVTZ basis set [with (2df, 2pd)-polarization] gave energies of similar quality to those obtained with set C and were therefore not considered further in this work.

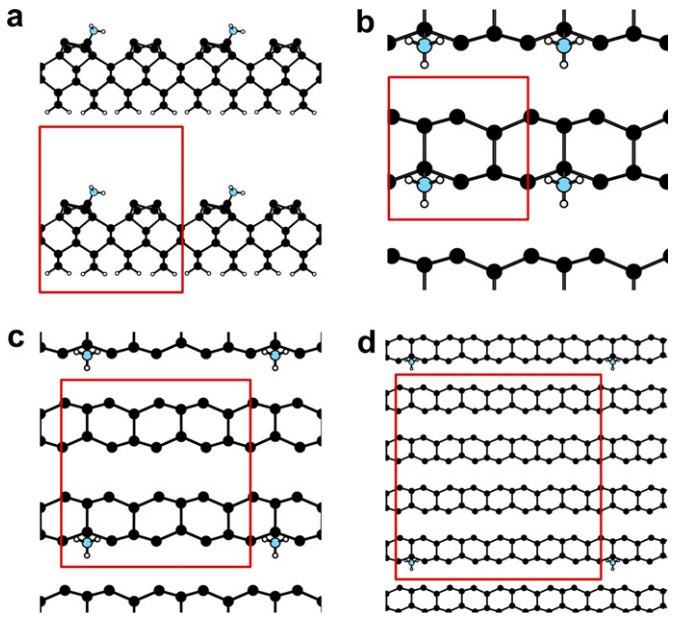

Fig. 3. Overview of slab models used in this work with the 3D periodic unit cells indicated by red rectangles: (a) side view of structure A1 (chemisorbed NH_3, *cf.* Fig. 1) on a slab with a p(4 × 4) surface unit cell, illustrating the stacking of successive slabs in the surface perpendicular direction. Panels (b–d) show top-views of structure A1 in p(2 × 2), p(4 × 4) and p(8 × 8) surface unit cell, respectively. In these top-view images, only adsorbed molecule and the two surface-nearest silicon layers are shown. Note that in all our calculations, we adopt the p(2 × 2) pattern of Si–Si dimer buckling. (For interpretation of the references to colour in this figure legend, the reader is referred to the web version of this article.)

surface, which are held fixed at silicon bulk positions, and a layer of terminating hydrogen atoms, which are also held fixed (similarly to the cluster termination) at a position along the broken Si–Si bond such that the Si(slab)–H bond length is 1.46 Å.[2] All other atoms in the slab are allowed to relax. The periodic cell dimensions were held fixed to the dimensions of the corresponding bulk-cell. Trial calculations conducted for the p(2 × 2) cell showed that a thickening of the slab to 14 Si-layers and a concomitant increase in the vacuum gap affected the calculated binding energies by less than 0.01 eV for the seven N + 3H structures considered. Convergence to less than 0.01 eV with respect to slab- and vaccum thickness was further confirmed in a single calculation [structure B10, p(2 × 2) cell] using a slab of 22 Si layers.

More critical in the calculation of molecular binding energies is the size of the surface unit supercell. With one molecule adsorbed per supercell, the size of the supercell determines the coverage of the surface with adsorbate molecules and thereby the separation between one adsorbate molecule and its periodic images. We will consider in the discussion section three supercell sizes: a p(2 × 2) cell (containing two dimers in one dimer-row), a (4 × 4) cell (eight dimers in two rows) and a p(8 × 8) cell (32 dimers in four rows). Integrations over the irreducible Brillouin zone (IBZ) were conducted using a Monkhorst and Pack [41] 4 × 4 × 1 **k**-point grid for the (2 × 2) surface slab model. This was reduced to a 2 × 2 × 1 grid for the p(4 × 4) surface unit cell model. In the p(8 × 8) cell calculations, the IBZ was sampled at the Γ-point only. Trial calculations using a denser 6 × 6 × 1 **k**-point grid for the p(2 × 2) cell resulted in binding energy changes of less than 0.01 eV for the seven trial structures, which indicates sufficient **k**-point convergence for our purpose. In the text we will also discuss planewave/pseudopotential calculations on cluster structures placed into large periodic cells with a minimum 8 Å vacuum between images. These calculations are **k**-point sampled at the Γ-point only.

We will further compare in the discussion section results obtained using three sets of atomic pseudopotentials[3] of increasing accuracy and computational cost (Table 3). The US-1 and US-2 sets are composed of Vanderbilt-type ultrasoft pseudopotentials [42,43], with the US-2 set using harder potentials than the US-1 set. A third set is based on projector augmented wave (PAW) potentials [44,45], which are regarded as being able to deliver energies of all-electron quality. The detailed composition of the three pseudopotential sets from the entries of the VASP pseudopotential library is given in Table 3. Calculations using the US-1 and US-2 potentials were performed using the recommended minimum planewave cutoffs of 225 eV and 350 eV, respectively. As we seek high accuracy with the PAW potential, we extended the planewave cutoff beyond the recommended minimum (400 eV) to 600 eV so as to achieve

[3] Here and in the following, our use of the collective word "pseudopotential" is inclusive of projector-augmented wave (PAW) potentials.

Table 3
Planewave/pseudopotential sets used in this work

Pseudopotential model	Nitrogen	Silicon	Hydrogen
US-1	N_s (225 eV)	Si (151 eV)	H_soft (150 eV)
US-2	N (348 eV)	Si (300 eV)	H_200 eV (200 eV)
PAW	N (400 eV)	Si_h (380 eV)	H (250 eV)

The individual atomic entries refer to the pseudopotentials in the VASP ultrasoft (US) and PAW-potential libraries [36,43,45]. Given in brackets for each atom are the library-recommended default cutoffs (in eV).

for this potential an estimated convergence of below 0.02 eV in binding energies with respect to planewave cutoff.[4] We did not extend the cutoff for the US-1 and US-2 potential beyond the recommended minimum cutoff for reasons that will become clear in the later discussion; we do, in essence, accept for these potentials an accuracy-loss due to a less-than-ideal cutoff, for the ability to run very large surface slab models [p(8 × 8) and p(4 × 4), respectively].

Finally, for both cluster and slab calculations, we emphasize that all energies reported for the seven trial structures are to be understood as *binding energies* relative to the isolated (gas phase) NH_3 molecule and the respective cluster or slab representing the free surface. This also applies to all energy corrections (e.g. cluster-size, slab-size, basis-set size, zero-point vibrational corrections) to be discussed below, which are all reported as corrections to the binding energy; thus combining the individual corrections for the separated and combined system. The advantage of focussing strictly on binding energies is that any systematic errors unrelated to the molecule–surface binding process are made to cancel.

3. Results

3.1. Testing basis set convergence – planewaves vs. Gaussians

We begin our discussion by directly comparing energies calculated by the planewave–pseudopotential and Gaussian-type orbital method for the seven trial structures using the same 3-dimer/small $Si_{21}H_{20}$ cluster representation of the surface. By focussing on the same cluster model in both methods, the principal purpose of these calculations is to establish the degree to which these rather different computational methods can achieve numerical agreement on calculated binding energy when the basis set and pseudopotential quality are increased. We calculate energies using the PW91 exchange–correlation functional in both methods, so any differences in the calculated energies reflect the basis set/pseudopotential approximations made.

Our results are summarized in Table 4. For the Gaussian cluster models, the increase of the basis set from our compact basis set A to basis set C results in a substantial changes of up to 0.15 eV in calculated energies. We note however that a single-point energy calculation using the C basis set at the geometry obtained with the A basis (this is denoted as C//A) reveals that most of the basis set effect is contained in the energy calculation, not in the geometry optimisation. The differences between the C//C and C//A energies are 0.02 eV or less, suggesting that basis set A is sufficient for geometry optimisations; thus, the effect of basis set increase on the energetics is adequately captured using single-point calculations with the larger basis. We further find that the difference between A//A and C//A (or C//C) is largely due to basis set superposition. This is evidenced by the single-point counterpoise correction evaluated for structure A1, which gives an estimate of the basis set superposition error of 0.08 and 0.02 eV for basis set A//A and C//A, respectively. With additional calculations using basis sets D//C and E//C, we seek to push closer towards the basis set limit. Significantly, the cc-pVQZ atomic basis set that is used within the D//C and E//C sets includes polarization functions going up to the g-level ($l = 4$) [33–35], one step higher than in C//C. The D//C results show that this increase continues to have an effect on calculated binding energies, amounting in the case of the G1 structure to 0.07 eV. Placing the cc-pVQZ basis set on all cluster atoms (basis set E//C) does not lead to any further changes of substance, illustrating that it is the near-surface atoms that are most in need of a large basis set. Note that calculations at the E//C level were not possible within our resources for structures B10 and C10, which lack any symmetry elements.

We now turn to the results obtained with the pseudopotential cluster models. While the US-1 model appears suitable to provide a rough qualitative ordering of the structure, there are considerable energy differences relative to the more accurate US-2 and PAW models. Structure G1 for instance differs by 0.46 eV in the energies calculated by US-1 and PAW. The US-2 model shows better agreement with the PAW model, but energy differences of up 0.21 eV remain in structure G1, which appears to emerge as a particularly stringent test structure for basis set dependence in both Gaussian and plane wave models. Structures C5 and C10 also exhibit differences of 0.09 eV between the US-2 and PAW models, highlighting the residual differences that the choice of pseudopotentials can have on the energetics. Whether the energies obtained with the PAW-600 eV potential are ''converged'' with respect to pseudopotential quality must remain a question of trust. For the planewave/pseudopotential model this represents the best model available to us.

By comparison of the respective best results from the Gaussian-type and planewave–pseudopotential models in Table 4 we can address the question to what extent these

[4] We adopt the general practice that the planewave cutoff for the augmentation charge density is three times the wavefunction cutoff. Convergence tests for this parameter are thus tied to those for the wavefunction cutoff.

Table 4
Basis set and pseudopotential dependence of the energies of NH_3 dissociation products

Model	Basis set	A1	B1	B6	B10	C5	C10	G1
Gaussians	A//A	−1.51	−2.20	−1.55	−0.68	−2.39	−1.74	−1.90
	B//B	−1.45	−2.11	−1.46	−0.61	−2.29	−1.66	−1.80
	C//A	−1.33	−2.07	−1.36	−0.54	−2.26	−1.68	−1.78
	C//C	−1.34	−2.05	−1.34	−0.54	−2.26	−1.68	−1.78
	D//C	−1.34	−2.08	−1.37	−0.57	−2.29	−1.71	−1.85
	E//C	−1.35	−2.07	−1.37	n/a	−2.28	n/a	−1.85
Planewaves	US-1 225 eV	−1.45	−2.34	−1.60	−0.82	−2.76	−2.18	−2.35
	US-2 350 eV	−1.38	−2.13	−1.41	−0.63	−2.41	−1.83	−1.68
	PAW 400 eV	−1.32	−1.98	−1.38	−0.57	−2.26	−1.68	−1.94
	PAW 500 eV	−1.36	−2.07	−1.38	−0.61	−2.33	−1.75	−1.88
	PAW 600 eV	−1.35	−2.06	−1.38	−0.63	−2.32	−1.74	−1.89
Difference PAW 600 eV–C//C		−0.01	−0.01	−0.04	−0.09	−0.06	−0.06	−0.11
Difference PAW 600 eV–D//C		−0.01	+0.02	−0.01	−0.06	−0.03	−0.03	−0.04

All energies are calculated using a 3-dimer/small cluster Fig. 2b and the PW91 GGA density functional. Gaussian basis sets and planewave/pseudopotentials are defined in Tables 2 and 3, respectively. For the Gaussian basis sets, the notation C//A indicates the basis sets used for energy calculation (basis C in this instance) and geometry optimisation (basis A).

rather different computational models can agree on energetics when all other parameters (i.e. cluster structure and density functional) are the same. The differences between GTO C//C and PAW-600 eV suggest that differences of up to 0.1 eV must be expected. Moving to the GTO D//C basis set reduces the differences to 0.04 eV for the structures considered. While this level of accuracy may be adequate for a given application, the following sections will show that the 3-dimer/small cluster is too small to be size-converged and that neither the PAW 600 eV pseudopotentials nor the D//C Gaussian-type model are practical for larger, size-converged cluster or slab models. We therefore now consider in turn the effects of cluster and slab size on energetics.

3.2. Effect of Gaussian cluster size on energetics

To study the effect of cluster size on energetics, we take a step back and consider first the compact and much less demanding A//A GTO basis set. The results are given in Table 5 and Fig. 4, where we have separated out the effects of extending a cluster in length (i.e. number of surface dimers) and bulkiness (width and depth). Looking first at the series of small clusters (*cf.* Fig. 2b) with dimer lengths from one to seven (Table 5 and Fig. 4b), one can observe a fairly rapid convergence with dimer length. With the exception of B10, all structures are converged to within 0.04 eV with the 3-dimer structure; B10 is converged with the 4-dimer cluster. The convergence is especially good

Table 5
Calculated energies (in eV) of NH_3 dissociation intermediates as a function of cluster size

Cluster		A1	B1	B6	B10	C5	C10	G1
Tiny	1-Dimer	−1.00	−2.08	−1.03	−0.44	−2.30	−1.68	−1.46
	3-Dimer	−1.35	−2.08	−1.27	−0.50	−2.25	−1.56	−1.89
Small	1-Dimer	−1.23	−2.38	−1.43	−0.75	−2.60	−1.95	−1.63
	2-Dimer	−1.42	−2.30	−1.53	−0.84	−2.52	−1.85	−1.88
	3-Dimer	−1.51	−2.20	−1.55	−0.68	−2.39	−1.74	−1.90
	4-Dimer	−1.50	−2.19	−1.56	−0.68	−2.40	−1.83	−1.89
	5-Dimer	−1.50	−2.18	−1.53	−0.70	−2.38	−1.86	−1.86
	6-Dimer	−1.51	−2.19	−1.54	−0.74	−2.39	−1.87	−1.87
	7-Dimer	−1.50	−2.18	−1.54	−0.75	−2.40	−1.87	−1.88
Large	1-Dimer	−1.25	−2.34	−1.38	−0.73	−2.55	−1.89	−1.44
	2-Dimer	−1.37	−2.22	−1.44	−0.80	−2.44	−1.77	−1.67
	3-Dimer	−1.47	−2.14	−1.46	−0.66	−2.33	−1.68	−1.69
	4-Dimer	−1.45	−2.13	−1.45	−0.65	−2.33	−1.78	−1.67
	5-Dimer	−1.44	−2.12	−1.43	−0.67	−2.32	−1.82	−1.66
	5-Dimer via Eq. (1)	*−1.46*	*−2.13*	*−1.44*	*−0.68*	*−2.32*	*−1.80*	*−1.64*
Extra large	3-Dimer	−1.46	−2.12	−1.44	−0.65	−2.30	−1.68	−1.71
Extra wide	3-Dimer	−1.58	−2.12	−1.46	−0.71	−2.31	−1.69	−1.70
Estimated limit	*Via Eq. (3)*	*−1.54*	*−2.09*	*−1.42*	*−0.75*	*−2.29*	*−1.85*	*−1.71*

All energy and geometry optimisations were performed at the Gaussian PW91/A level of theory. Estimated binding energies using extrapolation from smaller clusters (Eqs. (1) and (3), see text) are printed in italics; this includes our best-efforts estimate of cluster-size converged binding energies in the last row.

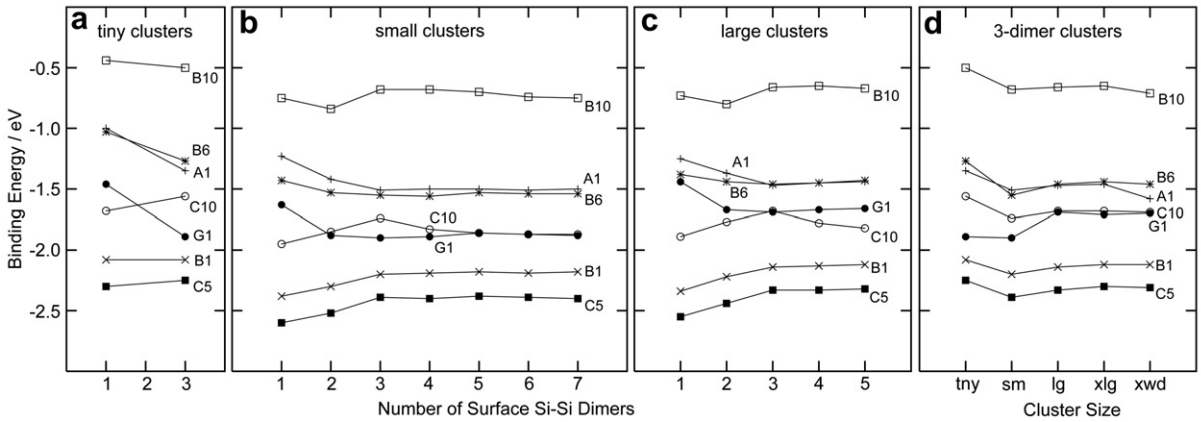

Fig. 4. Cluster-size dependence of the calculated binding energy (eV) of seven trial structures geometry optimised at the PW91/A level (*cf.* data in Table 5). For the cluster series *tiny*, *small*, and *large*, panels (a–c) show the dependence with respect to the length of the cluster, i.e. the number of the surface Si–Si dimers. Note how the individual structures show very similar cluster-length dependence between panels (a–c). This observation forms the basis of the additive cluster-size correction proposed in the text (Eq. (1)). Panel (d) shows the calculated binding energy for 3-dimer clusters of various thicknesses (tiny, small, large, extra-large and extra-wide).

for A1 and B1, which makes sense as these structures do not disrupt the free-surface bond connectivity, and are thus less prone to induce surface strain than the other structures. A very similar convergence with dimer-length can also be observed for the bulkier large clusters Table 5, Fig. 4c. While a comparison of the energies between small and large clusters reveals differences of up to 0.22 eV (in the G1 structure), we notice in Figs. 4b and c that the dependence with respect to dimer length of the large cluster series closely parallels that of the small series. Similarly, the trend between the 1- and 3-dimer clusters in the tiny cluster series Fig. 4a matches (though to a lesser extent) the trend seen in the small and large series Fig. 4b and c. This is useful because it suggests that we can estimate the effects of cluster lengthening and thickening as separate additive corrections. For example, the binding energies obtained with a 5-dimer/large cluster model could be approximated by the combination of the energies obtained with a 5-dimer/small cluster, a 3-dimer/large cluster and a 3-dimer/small cluster as follows:

$$\begin{aligned} &E(\text{5-dimer/large}) \\ &\quad \approx E(\text{3-dimer/small}) \\ &\qquad + [E(\text{5-dimer/small}) - E(\text{3-dimer/small})] \\ &\qquad + [E(\text{3-dimer/large}) - E(\text{3-dimer/small})] \end{aligned} \tag{1}$$

In this equation, the first term on the right side is the energy of the cluster upon which the extrapolation is based. The second and third terms in square brackets provide a *cluster-size correction* (*CSC*), i.e. a corrective term to account for the effects of cluster lengthening and widening, respectively. The extrapolated results for the 5-dimer/larger cluster are listed in Table 5 in italics alongside the directly calculated energies. How well this approximation works is further illustrated by the data in Table 6, where we have listed the energy difference between the left- and right-hand sides of Eq. (1) for analogous extrapolations from shorter/smaller to longer/larger clusters. The extrapolation from a 1-dimer/small cluster to a 5-dimer/large cluster introduces errors up to 0.07 eV. Extrapolating from the 2-dimer/small and 3-dimer/small cluster models reduces the largest error to 0.04 and 0.03 eV, respectively, and is thus at or below the chemical accuracy threshold. The benefit of this approach is that due to the steep scaling of CPU-time with respect to the number of atoms, the calculations on the three smaller or shorter clusters are much faster to run than a single long/large cluster calculation.

Before using the size extrapolation technique to arrive at a best-efforts estimate of cluster-size converged binding energies, we need to briefly consider the data in Fig. 4d showing the obtained binding energies for 3-dimer clusters with respect to cluster thickness (i.e. tiny, small, large, extra-large and extra-wide clusters). Good convergence with thickness is seen going up to the extra-large level (differences between 3-dimer/large and 3-dimer/extra-large clusters are 0.03 eV and below); however, two of the

Table 6
Calculated errors in the extrapolation to 5-dimer/large cluster energies by additive composition from smaller cluster models (Eq. (1))

Extrapolation	A1	B1	B6	B10	C5	C10	G1
1-Dimer/small → 5-dimer/large	+0.08	+0.03	+0.05	+0.02	+0.01	−0.02	+0.01
2-Dimer/small → 5-dimer/large	+0.01	−0.02	+0.01	−0.01	−0.02	−0.04	−0.01
3-Dimer/small → 5-dimer/large	+0.02	0.00	+0.01	+0.01	0.00	−0.02	−0.02
4-Dimer/small → 5-dimer/large	+0.01	+0.00	−0.02	+0.01	−0.01	+0.00	−0.02

Beginning with the 2-dimer/small cluster, the extrapolation errors are below the chemical accuracy level (0.04 eV).

structures (A1 and B10) experience a fairly substantial stabilization (0.12 and 0.06 eV, respectively) when going the extra-wide cluster. Recalling that the extra-wide cluster is the only cluster in our collection (Fig. 2) that includes adjacent dimer-rows, we can plausibly understand this additional stabilization as due to interactions with the adjacent dimer-row. In fact, both structure A1 and B10 feature polar N–H bonds that are directed with the H-end towards up-buckled (i.e. lone-pair carrying) dimer silicon atoms on the adjacent row and are thus prone to experience some form of additional electrostatic stabilization. The extra-wide cluster provides us with this important contribution.[5]

Combining now the energies obtained with our largest clusters, we can formulate an extrapolation to estimate the binding energies in the limit of very large cluster. We start with the energies obtained for the 5-dimer/large cluster and extrapolate (analogous to Eq. (1)) to a 7-dimer/large cluster using the difference between 7-dimer/small and 5-dimer/small. Two additional correction terms, account for the effects of extending cluster size to the extra-large and extra-wide level, including (via extra-wide) the important adjacent-row interactions.

$$\begin{aligned} &E(\text{estimated limit}) \\ &\quad \approx E(\text{5-dimer/large}) \\ &\qquad + [E(\text{7-dimer/small}) - E(\text{5-dimer/small})] \\ &\qquad + [E(\text{3-dimer/xlarge}) - E(\text{3-dimer/large})] \\ &\qquad + [E(\text{3-dimer/xwide}) - E(\text{3-dimer/large})] \end{aligned} \tag{2}$$

The resultant energies obtained for this 7-dimer/extra-large/extra-wide "super" cluster are listed in the last row of Table 5 and they represent our best estimate for PW91/A binding energies in the limit of a very large cluster.

Having arrived at an estimation of these cluster-size converged binding energies, we now seek to reduce the basis set error that is associated with using the small A basis set as opposed to, say, the larger C set. Recalling from the 3-dimer/small calculation above (Table 4) that C//C and C//A results differ by less than 0.02 eV, we expect that most of the basis set correction from A to C can be recovered without geometry reoptimization in a single-point C basis set calculation at the A basis set geometry. The calculated difference between C//A and A//A binding energies – in effect a *basis set correction* (*BSC*) – are listed in Table 7 and they can be seen to converge fairly rapidly with cluster size. For example, the basis set correction evaluated for the 3-dimer/small cluster differs by less than 0.03 eV from that obtained with the 5-dimer/large cluster. This suggests that the energy effect of basis set improvement may be captured using smaller clusters than required for achieving cluster-size convergence in the binding energy. Thus, we can establish cluster-size convergence using a compact basis set (e.g. basis set A) via the cluster-size extrapolation above (Eqs. (1) and (2)) and then apply an additional basis set correction evaluated using a smaller cluster (e.g. the 3-dimer/small cluster) to estimate PW91 binding energies for a large cluster and a large basis set.

3.3. Effect of planewave/pseudopotential slab size on energetics

Following on from the cluster models of the surface, we now discuss analogous size effects for surface slab models within the planewave/pseudopotentials representation of the surface. We consider three surface supercells of increasing size: $p(2\times2)$, $p(4\times4)$ and $p(8\times8)$ containing 2, 8 and 32 Si–Si dimers in 1, 2 and 4 dimer rows, respectively. In these three surface unit cells, the adsorbate species and their periodic images are increasingly separated by the cell repeat of 7.7, 15.4 and 30.9 Å, respectively, thus reducing any Coulomb- or strain-interactions between them. In Table 8, we have summarized our binding energy results obtained for these cell sizes with the different pseudopotential sets.

The results obtained for the same surface unit cell depend substantially on the quality of the pseudopotential set, with energy differences of up to 0.43 eV between US-1 and US-2 energies and up to 0.07 eV between US-2 and PAW-600 eV. This rather large dependence on the choice of pseudopotential/cutoff parallels our findings for the 3-dimer cluster above (Table 4). The higher accuracy provided by US-2 and PAW potentials however comes at increased computational cost with the effect that we were unable to run the largest cell [$p(8\times8)$] for the US-2 and PAW potentials and any but the smallest cell [$p(2\times2)$] for the PAW-600 eV. The $p(2\times2)$ cell however is not cell-size converged as is clearly illustrated by the US-1, US-2 and PAW-400 eV data. The US-1 $p(2\times2)$ energies differ by as much as 0.21 eV from those obtained using the large $p(8\times8)$ cell and the US-2 $p(2\times2)$ energies differ by up to 0.16 eV from the $p(4\times4)$ results. The $p(4\times4)$ cell is also not size converged as is shown by comparison with the $p(8\times8)$ energies for the US-1 potential where substantive energy differences of up to 0.07 eV occur. This takes us to the rather intriguing result in Table 9 showing the difference between $p(4\times4)$ and $p(2\times2)$ binding energies as obtained by the US-1, US-2 and PAW-400 eV potentials: All three potentials, including the US-1, agree to within a 0.01 eV margin on the effect of cell size increase from $p(2\times2)$ to $p(4\times4)$. This agreement is remarkable considering how much the potential models differ on the absolute binding energies. Thus, while the quality of the pseudopotentials is highly important for the accuracy of the binding

[5] The possibility of interaction of a surface adsorbate with the adjacent dimer row has practical implications on the choice of basis set. When using a composite GTO basis set of different quality depending on distance to the adsorbate (as detailed in Table 2), one might be tempted to place a compact, low-quality basis set (e.g. LANL2DZ) on the adjacent dimer-row. This however results for those adsorbate structures that do interact with the adjacent row in a substantial over-stabilization due to basis set superposition error. In our calculation, the basis set on the adjacent dimer-row atoms is the same (high quality) set as on the centre dimer-row.

Table 7
Binding energy difference E(PW91/C) − E(PW91/A) at the PW91/A geometry as a function of cluster size

Cluster		A1	B1	B6	B10	C5	C10	G1
Small	1-Dimer	+0.13	+0.14	+0.19	+0.15	+0.11	+0.10	+0.12
	3-Dimer	+0.17	+0.13	+0.19	+0.16	+0.12	+0.07	+0.12
	5-Dimer	+0.15	+0.13	+0.21	+0.13	+0.11	+0.05	+0.11
Large	3-Dimer	+0.14	+0.11	+0.18	+0.13	+0.10	+0.07	+0.10
	5-Dimer	+0.14	+0.12	+0.18	+0.16	+0.12	+0.07	+0.11

This data shows the rapid convergence of the A//A → C//A basis set correction (BSC) with cluster size.

Table 8
Calculated binding energies of NH_3 dissociation intermediates as a function of surface slab size and pseudopotential model

Method	Surface cell	A1	B1	B6	B10	C5	C10	G1
US-1 250 eV	p(2 × 2)	−1.42	−2.23	−1.47	−0.82	−2.65	−2.15	−1.99
	p(4 × 4)	−1.44	−2.23	−1.47	−0.93	−2.65	−2.28	−2.08
	p(8 × 8)	−1.46	−2.23	−1.47	−1.00	−2.65	−2.30	−2.12
US-2 350 eV	p(2 × 2)	−1.34	−2.03	−1.28	−0.62	−2.31	−1.81	−1.56
	p(4 × 4)	−1.36	−2.02	−1.28	−0.73	−2.31	−1.94	−1.65
PAW 400 eV	p(2 × 2)	−1.32	−1.99	−1.26	−0.61	−2.25	−1.76	−1.49
	p(4 × 4)	−1.34	−1.98	−1.26	−0.72	−2.25	−1.88	−1.59
PAW 600 eV	p(2 × 2)	−1.30	−1.96	−1.25	−0.63	−2.23	−1.73	−1.50
	p(8 × 8) via Eq. (3)	*−1.34*	*−1.95*	*−1.25*	*−0.82*	*−2.23*	*−1.88*	*−1.63*
	p(8 × 8) via Eq. (4)	*−1.33*	*−1.95*	*−1.25*	*−0.82*	*−2.23*	*−1.88*	*−1.63*

Values printed in italics are estimated PAW 600 eV p(8 × 8) energies obtained by one- and two-step extrapolation (Eqs. (3) and (4), respectively).

Table 9
Calculated energy difference E[p(4 × 4)] − E[p(2 × 2)] for three different pseudopotentials models

Method	A1	B1	B6	B10	C5	C10	G1
US-1 250 eV	−0.020	−0.001	+0.001	−0.112	−0.001	−0.126	−0.089
US-2 350 eV	−0.018	+0.005	+0.002	−0.108	0.000	−0.125	−0.093
PAW 400 eV	−0.018	+0.004	+0.001	−0.109	−0.001	−0.126	−0.091

While cell-size effects on binding energies are substantial for some of the structures (notably B10, C10 and G1), even the least-accurate US-1 model captures the energy difference to within 0.01 eV accuracy.

energy for a given cell size, even a low-quality potential/cutoff model can very adequately describe the extension from a smaller to a larger cell. The significance of this result is that we can use it to estimate binding energies for a high-quality potential (say, PAW-600 eV) and a prohibitively large cell [e.g. p(8 × 8)], by taking the high-quality results for a small cell [PAW-600 eV, p(2 × 2)] and use the low-quality US-1 potential to provide an additive size correction from p(2 × 2) to p(8 × 8), i.e.

$$\begin{aligned} &E(\text{PAW-600 eV}, \text{p}(8\times 8)) \\ &\quad \approx E(\text{PAW-600 eV}, \text{p}(2\times 2)) \\ &\qquad + [E(\text{US-1}, \text{p}(8\times 8)) - E(\text{US-1}, \text{p}(2\times 2))] \end{aligned} \tag{3}$$

In the following, we will refer to the second term in square brackets as a *slab size correction* (*SSC*). As in the case of the Gaussian cluster size expansion (Eq. 1) above, the computational benefit arises from the fact that cluster and slab size corrections involve several calculations at a lower level of basis set/pseudopotential quality that are more economical to compute than single large size, high-quality calculation. Let us briefly examine an alternative route to obtain the slab size correction from p(2 × 2) to p(8 × 8): In a two-step extrapolation, we may use the (arguably more accurate) PAW-400 eV results to correct from p(2 × 2) to p(4 × 4) and the US-1 results to correct from p(4 × 4) to p(8 × 8), i.e.

$$\begin{aligned} &E(\text{PAW-600 eV}, \text{p}(8\times 8)) \\ &\quad \approx E(\text{PAW-600 eV}, \text{p}(2\times 2)) \\ &\qquad + [E(\text{PAW-400 eV}, \text{p}(4\times 4)) \\ &\qquad - E(\text{PAW-400 eV}, \text{p}(2\times 2))] \\ &\qquad + [E(\text{US-1}, \text{p}(8\times 8)) - E(\text{US-1}, \text{p}(4\times 4))] \end{aligned} \tag{4}$$

As the results in Table 8 show, the one-step (Eq. (3)) and two-step (Eq. (4)) extrapolations give essentially the same energies; thus, little appears to be gained by the more involved two-step approach. Both equations provide us with a best-efforts estimate of the PW91 binding energy for a high-accuracy pseudopotential in the limit of a large surface unit cell.

3.4. Comparing size- and basis-set-converged cluster and slab models

In the previous two sections, we established in turn estimated binding energies using Gaussian cluster and slab models; the two models were extrapolated to large cluster/slab sizes, large basis sets and accurate pseudopotentials. An overview of these extrapolations and the individual steps involved is provided in Table 10. The differences between our best-efforts extrapolations for cluster and slab models are indicative of the residual error in the binding energies due to cluster/slab size and basis set/pseudopotential effects. With differences of +0.10 and −0.16 eV for structures A1 and B10, respectively, and between ±0.05 eV for the other structures, some structures are more affected by the size effects than others.

3.5. From GGA to B3LYP exchange–correlation

So far in our discussion all calculations were performed using the PW91 generalized gradient approximation (GGA) to the exchange–correlation energy, which is readily available in both Gaussian-type and planewave/pseudopotential implementations. It has, however, been recognized that the hybrid exact-exchange B3LYP density functional [31,32] provides on balance a more reliable representation of electron exchange and correlation materials as judged by comparison with high-level ab initio calculations and experimental molecular formation energies [31,46]. In Table 11, we report for our set of trial structures the binding energy difference $E(\mathrm{B3LYP}) - E(\mathrm{PW91})$ as a function of cluster-size. With differences up to 0.37 eV between the two functionals, it is clear that considerable energy uncertainties would remain if exchange–correlation corrections beyond the GGA were not applied. B3LYP calculations are substantially more demanding in computational cost than GGA functionals and display a less favourable scaling with system size. While this limits the application of the B3LYP model to smaller cluster/slab models than would otherwise be possible for the PW91 GGA model, this does not present a problem as a fairly rapid convergence of $E(\mathrm{B3LYP}) - E(\mathrm{PW91})$ with cluster size can be observed in Table 11. Thus we can use a B3LYP calculation conducted on a small cluster, to provide this difference as an exchange–correlation correction (XCC) for a large cluster, i.e.

$$\begin{aligned} &E(\mathrm{B3LYP}, \mathrm{large}) \\ &\quad \approx E(\mathrm{PW91}, \mathrm{large}) \\ &\qquad + [E(\mathrm{B3LYP}, \mathrm{small}) - E(\mathrm{PW91}, \mathrm{small})] \end{aligned} \tag{5}$$

Even the smallest, 1-dimer/tiny, cluster provides the difference term to within 0.06 eV to any of the other cluster sizes in the table. The 3-dimer/small cluster agrees to within 0.03 eV to the results obtained with the large 5-dimer/small

Table 10
Estimated system-size and basis-set limit for Gaussian cluster and planewave/pseudopotential slab models within the PW91 GGA approximation

		A1	B1	B6	B10	C5	C10	G1
Cluster	5-Dimer/large, PW91/A//A	−1.44	−2.12	−1.43	−0.67	−2.32	−1.82	−1.66
	CSC → 7-dimer/xlarge/xwide	−0.11	+0.04	+0.02	−0.09	+0.04	−0.03	−0.06
	BSC(3-dimer/small) → D//C	+0.11	+0.10	+0.18	+0.09	+0.06	+0.01	+0.03
	Total	−1.43	−1.99	−1.23	−0.66	−2.23	−1.83	−1.69
Slab	p(2 × 2), PAW-600 eV	−1.30	−1.96	−1.25	−0.63	−2.23	−1.73	−1.50
	SSC(US-1) → p(8 × 8)	−0.03	0.00	0.00	−0.19	0.00	−0.15	−0.13
	Total	−1.34	−1.95	−1.26	−0.82	−2.23	−1.88	−1.64
Difference E(Slab) − E(Cluster)		+0.10	+0.04	−0.02	−0.16	−0.01	−0.05	+0.05

All energies are given in eV. The Gaussian cluster extrapolation commences with the 5-dimer/large model and the A basis set (Table 5), to which is applied a three-step cluster-size correction (CSC, Eq. (2)) to estimate binding energies for a 7-dimer/extra-large/extra-wide cluster. An additional two-step basis set correction (BSC) based on the 3-dimer/small cluster is used to estimate PW91 binding energies at the D//C level. This involves, first a BSC to the C//A level (Table 7) and a second BSC correction to the D//C level using the energies in Table 4. The planewave slab model extrapolation proceeds via Eq. (3), based on the p(2 × 2) binding energies calculated using the PAW-600 eV pseudopotential set and the application of a slab-size correction (SSC) based on the US-1 potential to estimate PAW-600 eV results for a p(8 × 8) cell.

Table 11
The exchange–correlation correction E(B3LYP/A) − E(PW91/A) in eV as a function of cluster size

Cluster		A1	B1	B6	B10	C5	C10	G1
Tiny	1-Dimer	+0.14	−0.15	−0.19	−0.11	−0.35	−0.29	−0.31
	3-Dimer	+0.13	−0.13	−0.16	−0.06	−0.34	−0.26	−0.34
Small	1-Dimer	+0.12	−0.15	−0.19	−0.11	−0.35	−0.28	−0.30
	3-Dimer	+0.10	−0.16	−0.18	−0.05	−0.37	−0.26	−0.35
	5-Dimer	+0.10	−0.15	−0.17	−0.02	−0.35	−0.23	−0.36
Large	1-Dimer	+0.11	−0.16	−0.18	−0.11	−0.35	−0.30	−0.31
	3-Dimer	+0.10	−0.16	−0.17	−0.04	−0.36	−0.27	−0.34

All energies are calculated by geometry optimisation at the respective level of theory.

or 3-dimer/large clusters models; thus, a cluster of this size should suffice to deliver with good accuracy the desired correction from PW91 to B3LYP. Note that in our computation of this correction, we reoptimize the geometry at the B3LYP level. The rapid convergence of this correction with cluster size is intuitively consistent with the short-ranged nature of electron exchange and correlation. We further note that Hu et al. [47] in a very recent publication have reported a similar cluster size convergence for the CO molecule on the Cu(1 1 1) surface.

It is at this point worthwhile to briefly revisit basis set correction. In our discussion above we have applied the single point basis set correction at the PW91 level of theory, which was convenient in that it allowed us to directly compare PW91 results for size-converged slab and cluster models. If however, we extend the exchange–correlation model from PW91 to B3LYP using, say, a 3-dimer/small cluster, we find it more appealing to apply the basis set correction at the B3LYP level, and thereby correct basis set effects at the highest level of exchange/correlation. Further motivation comes from the observation that the basis set correction (Table 7) and the exchange–correlation correction (Table 11) appear to be of similar order of magnitude and rate of convergence with cluster size; suggesting that the same cluster be used for exchange–correlation and basis set correction. While the evaluation of the single-point basis set correction is computationally more expensive at the B3LYP level, the additional cost is small in comparison to the exchange–correlation and cluster-size corrections, which require geometry optimisation. Table 12, lists the B3LYP basis set correction for some of the cluster models used. While the trends in the data are similar to those obtained for PW91 (Table 7), the values are consistently lower.

3.6. Vibrational zero point energy

The importance of the zero-point vibrational energy is illustrated by the data in Table 13, where we list for our seven trial structures the calculated vibrational zero point correction (ZPC) to the binding energy as a function of cluster size. This correction was calculated using the Gaussian-type cluster model at the PW91/A level of theory. Ranging from −0.17 to +0.15 eV, the ZPC is clearly not a negligible quantity if energies with chemical accuracy are sought. Fortunately, the ZPC is seen to converge very rapidly with cluster size. Even when calculated using the simplest surface representation, the 1-dimer/tiny cluster, the obtained ZPC is to within 0.02 eV of the results for the largest cluster considered. Given the size of the correction, and the apparent ease with which it can be computed, there is no reason for not making it a routine component in the calculation of surface binding energies.

3.7. The combined model

We will now combine the size-extrapolated PW91 results for slab and cluster models with the exchange–correlation correction (XCC) and the vibrational zero-point correction to obtain our best-efforts binding energies. The PW91 cluster/slab-size and basis-set extrapolated results are taken from Table 10, to which the vibrational correction (ZPC) is added directly. The XCC contains an additional term to adjust the basis set correction already contained in the size-extrapolated cluster data of Table 10 so that the correction is applied at the B3LYP level, not the PW91 as discussed in Section 3.5 above. This leads – after some cancellation of terms – to the following expression for the XCC,

$$E_{\mathrm{XCC}} = [E(\mathrm{B3LYP/C//B3LYP/A}) - E(\mathrm{PW91/C//PW91/A})] \quad (6)$$

which is simply the difference between B3LYP and PW91 energies at the basis set corrected level (i.e. basis set C//A). All terms in the above equation are evaluated using the 3-dimer/small cluster. The correction is applied to both the cluster and slab models to give the final estimates for

Table 12
Basis set correction E(B3LYP/C) − E(B3LYP/A) at the B3LYP/A geometry as a function of cluster size

Cluster		A1	B1	B6	B10	C5	C10	G1
Small	1-Dimer	+0.11	+0.12	+0.17	+0.13	+0.08	+0.06	+0.10
	3-Dimer	+0.14	+0.10	+0.16	+0.12	+0.08	+0.02	+0.06
	5-Dimer	+0.14	+0.10	+0.16	+0.09	+0.06	+0.01	+0.09
Large	1-Dimer	+0.11	+0.12	+0.17	+0.15	+0.10	+0.09	+0.10
	3-Dimer	+0.10	+0.08	+0.18	+0.08	+0.05	+0.01	+0.01

Table 13
Calculated zero point vibrational corrections (ZPC, in eV) as a function of cluster size

Cluster		A1	B1	B6	B10	C5	C10	G1
Tiny	1-Dimer	+0.12	−0.01	+0.04	+0.05	−0.06	−0.05	−0.17
	3-Dimer	+0.13	+0.00	+0.05	+0.05	−0.05	−0.06	−0.16
Small	1-Dimer	+0.13	−0.01	+0.04	+0.05	−0.06	−0.06	−0.17
	3-Dimer	+0.14	+0.00	+0.06	+0.05	−0.05	−0.06	−0.15

The vibrational frequency calculations were performed at the PW91/A level of theory.

Table 14
Final composite binding energies for cluster and slab models: the PW91 basis-set and cluster/slab-size extrapolated results are taken from Table 10, to which are added the exchange–correlation correction (XCC, Eq. (6)) to the B3LYP level and the vibrational zero-point correction (ZPC)

		A1	B1	B6	B10	C5	C10	G1
Cluster	PW91 size-extrapolated	−1.43	−1.99	−1.23	−0.66	−2.23	−1.83	−1.69
Slab	PW91 size-extrapolated	−1.34	−1.95	−1.26	−0.82	−2.23	−1.88	−1.64
+	XCC (3-dimer/small)	+0.06	−0.19	−0.21	−0.13	−0.41	−0.31	−0.42
+	ZPC (3-dimer/small)	+0.14	+0.00	+0.06	+0.05	−0.05	−0.06	−0.15
Cluster	Total	−1.23	−2.17	−1.39	−0.68	−2.69	−2.20	−2.25
Slab	Total	−1.13	−2.14	−1.41	−0.84	−2.70	−2.25	−2.20
Difference E(Slab) − E(Cluster)		+0.10	+0.04	−0.02	−0.16	−0.01	−0.05	+0.05

Both XCC and ZPC terms were calculated using the 3-dimer/small cluster model.

the binding energies for the two models. As both the ZPC and XCC come from the cluster models, the residual differences between slab and cluster models (last row of Table 14) are of the course the same as those in the PW91 size-extrapolated results (Table 10), ranging between −0.16 (structure B10) and +0.10 eV (structure A1). The combined effect of XCC and ZPC causes shifts in the binding energies ranging between +0.20 (structure A1) and −0.57 eV (structure G1), highlighting the importance of these contributions relative to the residual cluster/slab size effects.

4. Discussion and conclusions

Taking the system NH_3 on Si(0 0 1) as an example, this account examined and contrasted two rather different approaches towards describing molecular species on a covalent surface: Gaussian cluster and planewave–periodic slab models. The premise of our discussion is that, ideally, these two models *should* agree on energetics and as a matter of practice do not. Contrasting the results obtained for both models as a function of four computational aspects (cluster/slab size, basis set size, exchange–correlation model, and vibrational zero point energy), we gain valuable insights into how both models are affected differently by the approximations made. In regard to the effect of finite cluster/slab size, we have observed no convincing evidence in our results that periodic slab models are intrinsically superior to non-periodic cluster models (and vice versa). Both suffer from substantive finite system size effects that extend to fairly large cluster and unit cell sizes (Tables 5 and 8). In both models these finite size effects can be alleviated using additive cluster/slab size correction terms (e.g. as used in Eqs. (1)–(4)) evaluated at a lower/faster level of theory. The chief weakness of the Gaussian cluster models appears to rest with their limits to basis set completeness, which, in contrast, is a strength of the planewave model (provided a good pseudopotential is used). It has been previously noted in the context of molecular calculations [48–50], that planewave/pseudopotential basis sets are very competitive (in accuracy) with highest-level Gaussian basis sets. We fully concur with these earlier observations in that it was only with the very large cc-pVQZ basis set (i.e. set D; polarization functions up angular momentum $l = g$) that a desirable degree of numerical agreement between Gaussian basis and planewave results was achieved (Table 5). This basis set, however, is impractical for all but the smallest of clusters. Yet, the results show that the ability of a basis set to describe atomic polarization to high angular momentum ($l = d, f, g\ldots$) is clearly important for accurate energetics. Unlike planewaves, which naturally (and economically) extend to high-l values, GTO basis sets are limited by the extent such functions are included in the atomic sets. However, in the GTO basis sets also rests the greatest strength of the Gaussian cluster model approach in that electron-exchange can be evaluated analytically, permitting the routine use of the superior B3LYP functional. It is clear from Table 14 that the XCC (i.e. the energy difference between B3LYP and PW91) is easily of the same significance as cluster/slab size effects, basis set/pseudopotential, vibrational zero-point effects. Not explored here were levels of theory beyond DFT (e.g. multiconfigurational SCF, coupled-cluster theories and quantum Monte-Carlo) however these advanced methods too appear more readily accessible for Gaussian basis sets rather than planewave sets. The results present in this work provide support to the idea of using compound models to improve the accuracy of calculated binding energies of molecules on surfaces. As in gas-phase quantum chemistry (e.g. Refs. [21–23]), we combine several calculations to economically estimate binding energies at higher level of exchange–correlation and basis set completeness. We also show that a similar compounding approach can also be used to estimate binding energies for large clusters and slab models. Finally, this work highlights the advantages of using Gaussian cluster and planewave–periodic models in parallel. The very difference of the two approaches reveals the strengths and limitations of both. This could be further exploited in compound models involving the two approaches in combination to achieve higher accuracy in calculated binding energies.

Acknowledgements

This work was supported by the Australian Research Council, the Australian Government, the US Advanced Research and Development Activity, National Security Agency, and Army Research Office under Contract No. DAAD19-01-1-0653. Computing support was provided by the Australian Partnership for Advanced Computing (APAC).

References

[1] M.A. Filler, S.F. Bent, Prog. Surf. Sci. 73 (2003) 1.
[2] J. Yoshinobu, Prog. Surf. Sci. 77 (2004) 37.
[3] C. Africh, G. Comelli, J. Phys.: Condens. Matter 18 (2006) R387.
[4] X. Lu, M.C. Lin, Int. Rev. Phys. Chem. 21 (2002) 137.
[5] Silicon nitride in electronics, in: V.I. Belyi (Ed.), Materials Science Monographs, vol. 34, Elsevier, New York, 1988.
[6] X. Xu, S.-Y. Kang, T. Yamabe, Phys. Rev. Lett. 88 (2002) 076106.
[7] X. Xu, S.-Y. Kang, T. Yamabe, Chem. Eur. J. 8 (2002) 5351.
[8] Y. Widjaja, C.B. Musgrave, Phys. Rev. B 64 (2001) 205303.
[9] T.L. McDonell, N.A. Marks, O. Warschkow, H.F. Wilson, P.V. Smith, M.W. Radny, Phys. Rev. B 72 (2005) 193307.
[10] H.-J. Kim, J.-H. Cho, Phys. Rev. B 69 (2004) 233402.
[11] E. Fattal, M.R. Radeke, G. Reynolds, E.A. Carter, J. Phys. Chem. B 101 (1997) 8658.
[12] Y. Widjaja, M.M. Mysinger, C.B. Musgrave, J. Phys. Chem. B 104 (2000) 2527.
[13] Y. Widjaja, C.B. Musgrave, Surf. Sci. 469 (2000) 9.
[14] Y. Widjaja, C.B. Musgrave, J. Chem. Phys. 120 (2004) 1555.
[15] R. Miotto, G.P. Srivastava, R.H. Miwa, A.C. Ferraz, J. Chem. Phys. 114 (2001) 9549.
[16] S.-H. Lee, M.-H. Kang, Phys. Rev. B 58 (1998) 4903.
[17] O.N. Chung, H. Kim, S. Chung, J.-Y. Koo, Phys. Rev. B 73 (2006) 033303.
[18] J.H.G. Owen, D.R. Bowler, S. Kusano, K. Miki, Phys. Rev. B 72 (2005) 113304.
[19] J.-Y. Lee, J.-H. Cho, J. Phys. Chem. B 110 (2006) 18455.
[20] Z.K. Smedarchina, M.Z. Zgierski, Int. J. Mol. Sci. 4 (2003) 445.
[21] L.A. Curtiss, K. Raghavachari, G.W. Trucks, J.A. Pople, J. Chem. Phys. 94 (1991) 7221.
[22] J.A. Montgomery Jr., J.W. Ochterski, G.A. Petersson, J. Chem. Phys. 101 (1994) 5900.
[23] J.W. Ochterski, G.A. Petersson, J.A. Montgomery Jr., J. Chem. Phys. 104 (1996) 2598.
[24] P. Nachtigall, K.D. Jordan, A. Smith, H. Jonsson, J. Chem. Phys. 104 (1996) 148.
[25] E. Penev, P. Kratzer, M. Scheffler, J. Chem. Phys. 110 (1999) 3986.
[26] J.A. Steckel, T. Phung, K.D. Jordan, P. Nachtigall, J. Phys. Chem. B 105 (2001) 4031.
[27] C. Filippi, S.B. Healy, P. Kratzer, E. Pehlke, M. Scheffler, Phys. Rev. Lett. 89 (2002) 166102.
[28] M.J. Frisch, G.W. Trucks, H.B. Schlegel, G.E. Scuseria, M.A. Robb, J.R. Cheeseman, J.A. Montgomery, Jr., T. Vreven, K.N. Kudin, J.C. Burant, J.M. Millam, S.S. Iyengar, J. Tomasi, V. Barone, B. Mennucci, M. Cossi, G. Scalmani, N. Rega, G.A. Petersson, H. Nakatsuji, M. Hada, M. Ehara, K. Toyota, R. Fukuda, J. Hasegawa, M. Ishida, T. Nakajima, Y. Honda, O. Kitao, H. Nakai, M. Klene, X. Li, J.E. Knox, H.P. Hratchian, J.B. Cross, V. Bakken, C. Adamo, J. Jaramillo, R. Gomperts, R.E. Stratmann, O. Yazyev, A.J. Austin, R. Cammi, C. Pomelli, J.W. Ochterski, P.Y. Ayala, K. Morokuma, G.A. Voth, P. Salvador, J.J. Dannenberg, V.G. Zakrzewski, S. Dapprich, A.D. Daniels, M.C. Strain, O. Farkas, D.K. Malick, A.D. Rabuck, K. Raghavachari, J.B. Foresman, J.V. Ortiz, Q. Cui, A.G. Baboul, S. Clifford, J. Cioslowski, B.B. Stefanov, G. Liu, A. Liashenko, P. Piskorz, I. Komaromi, R.L. Martin, D.J. Fox, T. Keith, M.A. Al-Laham, C.Y. Peng, A. Nanayakkara, M. Challacombe, P.M.W. Gill, B. Johnson, W. Chen, M.W. Wong, C. Gonzalez, J.A. Pople, Gaussian 03, Revision D.01, Gaussian Inc., Wallingford CT, 2004.
[29] J.P. Perdew, in: P. Ziesche, H. Eschrig (Eds.), Electronic Structure of Solids '91, Akademie Verlag, Berlin, 1991, p. 11.
[30] J.P. Perdew, J.A. Chevary, S.H. Vosko, K.A. Jackson, M.R. Pederson, D.J. Singh, C. Fiolhais, Phys. Rev. B 46 (1992) 6671.
[31] A.D. Becke, J. Chem. Phys. 98 (1993) 5648.
[32] C. Lee, W. Yang, R.G. Parr, Phys. Rev. B 37 (1988) 785.
[33] T.H. Dunning Jr., J. Chem. Phys. 90 (1989) 1007.
[34] R.A. Kendall, T.H. Dunning Jr., R.J. Harrison, J. Chem. Phys. 96 (1992) 6796.
[35] D.E. Woon, T.H. Dunning Jr., J. Chem. Phys. 98 (1993) 1358.
[36] G. Kresse, J. Hafner, J. Furthmüller, VASP (Vienna Ab Initio Simulation Package), Version 4.6, Institut für Materialphysik, Universität Wien, Vienna, 2003.
[37] G. Kresse, J. Hafner, Phys. Rev. B 47 (1993) 558.
[38] G. Kresse, J. Hafner, Phys. Rev. B 49 (1994) 14251.
[39] G. Kresse, J. Furthmüller, Comput. Mater. Sci. 6 (1996) 15.
[40] G. Kresse, J. Furthmüller, Phys. Rev. B 54 (1996) 11169.
[41] H.J. Monkhorst, J.D. Pack, Phys. Rev. B 13 (1976) 5188.
[42] D. Vanderbilt, Phys. Rev. B 41 (1990) 7892.
[43] G. Kresse, J. Hafner, J. Phys.: Condens. Matter 6 (1994) 8245.
[44] P. Blöchl, Phys. Rev. B 50 (1994) 17953.
[45] G. Kresse, D. Joubert, Phys. Rev. B 59 (1999) 1758.
[46] L.A. Curtiss, K. Raghavachari, P.C. Redfern, J.A. Pople, J. Chem. Phys. 112 (2000) 7374.
[47] Q.-M. Hu, K. Reuter, M. Scheffler, Phys. Rev. Lett. 98 (2007) 176103.
[48] S.B. Andrews, N.A. Burton, I.H. Hillier, J.M. Holender, M.J. Gillan, Chem. Phys. Lett. 261 (1996) 521.
[49] R.J. Meier, J. Mol. Struct. (Theochem) 467 (1999) 79.
[50] L. Fusti-Molnar, P. Pulay, J. Chem. Phys. 116 (2002) 7795.